Synthesis of a Novel Supermagnetic Fe_3O_4 Nanoparticles and their Congo Red Dye Removal, Cytotoxic, Antioxidant, and Antimicrobial Activities

Semih GÖKDAĞ
Fatma CAF
Fulya DOĞANER
BÜLENT KAYA (b_kaya_tr@yahoo.com)
Bingöl Üniversitesi https://orcid.org/0000-0002-1216-6441
Adnan AYNA
Gürkan AYKUTOĞLU

Research Article

Keywords: Anticancer, Antimicrobial, Congo red, Fe nanoparticles, Langmuir Isoterm, Plantago lanceolata

Posted Date: March 21st, 2022

DOI: https://doi.org/10.21203/rs.3.rs-1458659/v1

Abstract

Biogenic synthesis of iron nanoparticles has been reported in many studies. However, there is no such study that combines antioxidant, antimicrobial, anticancer and dye removal activities of the synthesized iron nanoparticles. The present study focused on the green synthesis and Congo Red (CR) dye removal, cytotoxic, antioxidant and antimicrobial activities of supermagnetic Fe_3O_4 nanoparticles using *Plantago lanceolata* L. extracts (PLE@FeNPs). The morphology and physical properties of PLE@FeNPs were characterized by FTIR, XRD, SEM, EDX, TEM and DLS analysis. XRD and zeta potential analysis revealed a potential of-12.2 mV and formation of cubic crystals, with an average dimension of 7 nm, and a wide band at 352 nm was detected in UV-vis spectroscopy. The optimum adsorption conditions of pH, temperature and adsorbent amount for CR removal were found as pH 4, 25 ℃ and 15 mg respectively with a high removal efficiency of 99 %. To evaluate dye adsorption behaviors of the PLE@FeNPs, adsorption isotherm models -Langmuir, Freundlich and Temkin- were applied to the present data. Langmuir Isotherm model (R^2 = 0.96, 25 °C) were best fitted to our data. Thermodynamic evaluation of the results showed that the reaction was spontaneous (ΔG = -26.6 kJ mol^{-1}) and exothermic (ΔH -35, 3 kJ mol^{-1}). PLE@FeNPs showed highest antimicrobial activity on *Staphylococcus aureus.* Antioxidant activities of PLE@FeNP was examined by DPPH removal (89.79%) and metal-chelating activity (74%). The *in vitro* cytotoxicity experiments showed that PLE@FeNPs possessed significant cytotoxic effects in human lung cancer (A549) cell line while no such effects were observed on human neuroblastoma (SH-SY5Y) cell line. PLE@FeNPs also caused DNA fragmentation on A549 cells. Overall these results pave the way for further applications in dye removal and biological applications of environmentally friendly PLE@FeNPs.

1. Introduction

Nanotechnology is the science that deals with the synthesis of particles between 1-100 nm sizes. Physical production, bottom-up production synthesis and top-down synthesis method were used as chemical methods for the synthesis of nanoparticles. However, these methods have high costs, cause environmental pollution, and release of toxic agents. The easy, inexpensive, environmentally friendly biological green synthesis method has emerged as a synthesis route with increasing interest in recent years [1]. In particular, the potential and inimitable physicochemical properties of metal nanoparticles, unique smallness, size, electrooptic, catalytic, thermal resistance, surface area properties make nanoparticles suitable candidates for many purposes [2–4]. NPs in particular have shown broad-spectrum antibacterial, antioxidant, anticancer activities [5–9].

The increasing population, changes and diversity in production processes and environmental changes that accompany industrial development endanger the quality of water and cause increased water contamination [10]. Synthetic dyes, are the primary causes of water pollution [11]. Studies have shown that artificial dyes can bind to the DNA and proteins inside cells and causes severe health problems

including cancer [12]. Therefore, the removal of these dye components from water has become a major research area.

Scientists have developed several methods for cleaning water to remove the dye wastes. These methods include reverse osmosis, chemical precipitation, ion exchange and electrocatalysis. However, the application of these methods is hindered by low efficiency, high energy consumption, and toxicity. Extensive research is being carried out to develop alternative methods to overcome these problems [10]. Adsorption is a simple, economical process with a high processing efficiency and reusability of the adsorbents for dye removal from the wastewater. Interest in the field of nano-adsorbents has increased as the conventional adsorbents have limited efficiency, with low surface or active area, lack of selectivity, and adsorption kinetics [13]. The selectivity for surface area or volume in nano-adsorbents is better than traditional adsorbents. Iron oxide nanoparticles are one of the most widely used nanomaterials due to the simplicity of their synthesis and their ability to remove a large number of pollutants, alone or in combination with other adsorbents [14].

Iron nanoparticles (FeNPs) have several applications including drug targeting in cancer therapy [7, 15], antioxidant [5, 16], anticancer [17, 18], antimicrobial [19–22], dye removal and degradation [3, 22, 23, 24]. The reports have shown that they have high efficiency, wide distribution ranges and low cost in removing pollutants in treatment processes [25]. Plantago is a large genus of the Plantaginaceae family which are rich in iridoids, iridoid glycosides, flavonoids, polysaccharides, polyphenols, and triterpene acid content. They have been used as alternative medicines in the treatment of wound healing, diabetes, infection, cancer, and intestinal problems. Plantago members are also used in the food industry in some countries [26]. These plants are widely used in the pharmaceutical industries, as studies have shown that Plantago has high antioxidant, anticancer, antibacterial, antifungal, antiviral and anti-inflammatory activities [27]. However, there is no study combining experiments such as antioxidant, antimicrobial, anticancer and dye removal activities of supermagnetic FeNPs of *Plantago lanceolata* L. in the literature.

In the current study, we report the biosynthesis of *Plantago lanceolata* L. (ribwort) leaf extract mediated FeNPs for the first time. The physicochemical parameters of the synthesized PLE@FeNPs were evaluated by employing several analytical techniques owing to the fact that the size, shape, and stability of the nanoparticles greatly affect their biological properties [28]. The *in vitro* biological activities (antimicrobial, antioxidant, cytotoxic) and Congo Red removal activities of PLE@FeNPs were further analyzed.

2. Materials And Methods

2.1. Chemicals

All chemicals were obtained from Aldrich and Merck. Chemicals used in the present study are as follows: iron chloride tetrahydrate ($FeCl_2{\cdot}4H_2O$), iron chloride hexahydrate ($FeCl_3{\cdot}6H_2O$), sodium hydroxide (NaOH), hydrochloric acid (HCl), Congo red ($C_{32}H_{22}N_6Na_2O_6S_2$), ethanol ($C_2H_5OH$), methanol ($CH_3OH$), hydrogen peroxide ($H_2O_2$), dimethyl sulfoxide ($C_2H_6OS$), sodium carbonate ($Na_2CO_3$), Folin-Ciocalteu

reagent, sodium nitrite ($NaNO_2$), aluminum chloride ($AlCl_3$), DPPH ($C_{18}H_{12}N_5O_6$), ferrozine ($C_{20}H_{12}N_4Na_2O_6S_2$), sulfuric acid ($H_2SO_4$), monosodium phosphate (NaH_2PO_4), and ammonium molybdate ($(NH_4)_6Mo_7O{\cdot}4H_2O$).

2.2. Collection of plant material

Plantago lanceolata L. leaves were collected from Aksaray University campus between November and December 2019. Species were identified by Prof. Dr. Lütfı Behçet from Bingöl University, Faculty of Arts and Sciences, Biology Department. The collected leaves were separated from the branches, washed with water and dried in the shade.

2.3. Extraction of *P. lanceolata* plant (PLE)

First, the leaves of the dried *P. lanceolata* (ribwort) plant were ground. Then, 35 g of the ground plant was weighed, and 350 mL of distilled water was added (to a ratio of 1/10). The prepared plant solution was kept at 20°C on a magnetic stirrer for approximately 24 hours. After 24 hours, the plant solution was removed from the magnetic stirrer and filtered. Due to evaporation, the volume was reduced to around 250 mL, which was much too concentrated, therefore distilled water was added to bring the solution back up to 350 mL.

2.4. Iron nanoparticle (FeNP) synthesis by *P. lanceolata* (PLE@FeNPs)

Initially 100 mL of $FeCl_2{\cdot}4H_2O$ (0.01 M) and $FeCl_3{\cdot}6H_2O$ (0.01 M) were prepared. Then, they were mixed and heated at 60°C on a magnetic stirrer. After the temperature of this mixture was fixed, 200 mL of plant extract (PLE/water = 1:10) was added and mixed at 200 rpm. After 30 minutes, 20 mL of NaOH (2M) was slowly dripped into the mixture. Following the dripping process, the mixture was stirred for another 40 minutes (60°C, 200 rpm). Then, the nanoparticles, which precipitated at room temperature, were washed three times with 200 mL water and twice with 200 mL ethanol to remove chlorine residues. Subsequently, PLE@FeNPs were dried in a glass petri dish at 40°C.

2.5. Adsorption experiments

Congo red (CR) adsorption experiments were performed using synthesized PLE@FeNPs. The effects of pH, dye concentration, adsorbent concentration and adsorption temperature on CR adsorption were investigated. After the adsorption process, dye concentrations in the solutions were determined by measuring absorption at 538 nm. First, dye removal was studied at different pH levels. A solution of Congo red (CI name = Direct Red 28, CI No. = 22120, $C_{32}H_{22}N_6O_6S_2Na_2$, formula weight = 696.65) was prepared by mixing 200 ppm of Congo red (28.7 mmol) with 100 mL of distilled water at ambient temperature. Other concentrations were prepared by diluting this stock dye (200 ppm) solution. For each concentration, the pH range of 2–8 was studied. For Fenton reaction, 10.0% H_2O_2 solution (v/v) was prepared by diluting 30.0% H_2O_2 solution (Merck 64271) with deionized water, and 1 mL of 10.0% H_2O_2 solution was added to all test sets. Then, 200 µl samples were taken from each set before and after the

adsorption process and transferred to a 96-well plate. The absorbance measurements at 538 nm were recorded.

The adsorption capacity and removal efficiency of the biosorbent at equilibrium were calculated using equations (1) and (2), respectively:

$$qe = \frac{Ci\text{-}Ce}{W} \times V$$

1

$$\text{Adsorption (\% removal efficiency)} = \frac{Ci\text{-}Ce}{Ci} \times 100$$

2

The equations commonly used to define the adsorption isotherm are the Langmuir, Freundlich, and Temkin equations, which were used in this study. With the help of these equations, the surface properties of the adsorbent and the relationship between adsorbent and adsorbed material can be defined. Kinetic data were modeled using the pseudo-first-order (PFO) model [29] and the pseudo-second-order (PSO) model [30](Ho and McKay, 1999).

2.6. Determination of biological activities of PLE@FeNPs

2.6.1. Antioxidant activity

For the determination of antioxidant activity, 1 mg/mL of PLE@FeNPs and 2 mL of *P. lanceolata* extract were used. The experiments were repeated three times. Total phenol content was calculated per kilogram as gallic acid equivalents using the method of Folin and Ciocalteu [31]. Total flavonoid content [32], total antioxidant capacity [33], DPPH radical effect [34], and metal chelating activity [35] of PLE@FeNPs and *P. lanceolata* were determined. All samples were transferred to a 96-well plate, and absorbance was measured at 695 nm in ELISA for antioxidant activity.

2.6.2 Cytotoxic activity

A549 (human lung cancer cell line) and SH-SY5Y (human neuroblastoma cell line) cells used in the study were obtained from Bingöl University, Department of Molecular Biology and Genetics. The cells were stored at -80°C prior to use.

Cytotoxic activities of PLE@FeNPs and plant extract of *P. lanceolata* L were studied against A549 and SH-SY5Y cell lines using MTT assay. The cells were cultured in Dubelco's Modified Eagle Medium (DMEM) supplemented with 10% Fetal Bovine Serum (FBS) and streptomycin; penicillin (100 µg/mL). The cells were maintained in humidified CO_2 incubator with 5% CO_2 and 95% humidity for 48 hours. The cells were seeded in 96 well tissue culture plates along with different concentration of PLE@FeNPs (30–1000

µg/mL) and incubated for 72 hours. After 72 hours of incubation, 20 µL of MTT was added into the each well and incubated at 37°C for 4 hours and absorbance values at 450–690 nm were measured.

2.6.3. DNA fragmentation activity

The DNA fragmentation assay was performed based on the slight modification of Tartik et al., 2016 [36]. The cells (A549 and MRC-5) were cultured and treated as explained in section 2.6.2. After PLE@FeNPs (1 mg/mL) treatment, cells were collected and washed with PBS. Afterwards, the cells were centrifuged at 4000 rpm for three min. The obtained pellet was suspended with DNA lysis buffer and incubated on ice for an hour and DNA isolation was performed following the procedure supplied with content (Biospeedy, Turkey). DNA concentration was measured at 260 nm using a spectrophotometer (Shimadzu, Japan). DNA was run on a 1.5% agarose gel (containing 3 mg/mL ethidium bromide in 1xTAE buffer of pH 8.5) at 90 V for 45 minutes and bands were visualized using a UV transilluminator (BioRad USA).

2.6.4. Antimicrobial activity

Microorganisms used for antimicrobial activity were obtained from Refik Saydam Public Hygiene Center. The organisms used in the study were gram-positive (+) microorganisms *Staphylococcus aureus* (ATCC 29213); gram-negative (-) microorganisms *Klebsiella pneumoniae* (EMCS) and *Escherichia coli* (ATCC 25922), and yeast *Saccharomyces cerevisiae*. Antimicrobial activities were measured by ELISA reader.

Antimicrobial activities of both nanoparticles and plant extracts were studied by microdilution approach in 96-well plate. The bacteria cultures were incubated overnight in Mueller Hinton Broth and diluted as Mc Farland 0.5 ($1–2 \times 10^5$). Following that, the cells were mixed with serially diluted PLE@FeNPs and plant extract of *P. lanceolata* L with the final concentration ranging from 0.15625 mg /mL to 5 mg /mL. After incubation at 35.5°C for 24 h, the optical density at 538 nm was determined and MIC values were calculated.

2.6.5 Statistical Analysis

All experiments were performed in triplicate. Statistical analysis was carried out GraphPad Prism 5.01 software and comparable data groups were evaluated by one-way ANOVA post hoc Tukey's test; $p < 0.05$ was considered as significant.

3. Results And Discussion

3.1 Characterization

The formation of PLE@FeNPs was examined and confirmed via UV-vis spectroscopy to evaluate the signature surface plasmon resonance (SPR) bands. The UV–Vis absorption analysis re-vealed the broad band at around 352 nm (Fig. 1a), A single SPR band indicates the formation ıf spherical nanoparticles, while presence of two or more SPR bands indicates formation of anisotropic molecules [37]. There is a possibility that the different absorptions may be due to the various components of the plant extracts. The

bands observed around 204 nm and 352 nm were due to the surface plasma resonance created by iron electrons (Fig. 1a).

FT-IR analysis was performed to determine the surface chemistry of P. lanceolata L. plant extract and PLE@FeNPs, and functional groups present in the active ingredients were identified (Fig. 2b). In the FT-IR analysis of PLE@FeNP, peaks with values of 983 cm^{-1}, 1146 cm^{-1}, 1463 cm^{-1}, 1578 cm^{-1}, 1726 cm^{-1}, 2932 cm^{-1}, and 3444 cm^{-1} were obtained. The peak of the broad and dense band formed by organic compounds with hydroxyl (OH) groups in the plant extract occurred at 3444 cm^{-1} [38, 39]. The 2932 cm^{-1} band indicated the presence of aliphatic hydrocarbons with CH and CH_2 groups [40]. The band at 1726 cm^{-1} originated from the C-O, C-H, and C = C groups of aromatic compounds [41]. The band at 1578 cm^{-1} formed due to C = C aromatic ring stretching vibration [40]. It has been observed that bands of C-H, C-O and C = C groups of water-soluble organic compounds are formed at 1463 cm^{-1}, 1146 cm^{-1} and 983 cm^{-1} [42]. The bands formed indicated that the organic groups cover the surface of the nanoparticles and keep them stable. The presence of functional groups (aromatics, phenols, amines, hydroxyl groups, carboxyl groups, carbonyl groups, and aliphatic hydrocarbon groups) in the structure of the P. lanceolata extract were confirmed based on the observed bands [40, 43].

The crystal structure and phase of PLE@FeNPs were characterized by XRD (Fig. 1c). XRD spectrum of the nanoparticles revealed the presence of distinct diffraction peaks at 2θ = 38°, 44.9°, 47.1°, 54.9°, 68.9°, 73.9°, 81.7° and 93.4°. The obtained peaks were determined to be the characteristic of magnetite [44–46]. The indexes corresponding to these peaks are (220), (311), (222), (400), (422), (511), (440) and (620), respectively. These are the peaks of iron oxide in the crystal structure, and these peaks are the magnetite (Fe_3O_4) form of the synthesized nanoparticles. This analysis fits the PLE@FeNP reference model (JCPDS: 00-001-1111/ cubic).

TEM images showed that most of the PLE@FeNPs were spherical, and histogram calculations show the average size of the nanoparticles obtained in the TEM images was 8 nm (Fig. 1d). The morphological structure of PLE@FeNPs were investigated using TEM (Fig. 1e). The thin layer surrounding the PLE@FeNPs supports the presence of plant metabolites in the *P. lanceolata* extract that reduce Fe ions to nanoparticles.

The electrical charge of the synthesized PLE@FeNPs was determined by zeta potential analysis (Fig. 1f). The zeta potential, a measure of the charge on the surface of nanoparticles, indicates the electrical potential of moving nanoparticles [47]. The zeta potential showed that PLE@FeNPs have an electrical charge of − 12.2 mV. This value indicates that PLE@FeNPs are moderately stable [48, 49]. A negative value may occur due to the adhesion of organic compounds to the surface of iron nanoparticles [50].

The sizes and morphological structures of PLE@FeNPs were examined using SEM (Fig. 1g). The results obtained from the SEM images showed the aggregation of PLE@FeNPs. The functional groups in the plant extract used have an effect on the formation of this morphological structure [51]. Elements in the structure of PLE@FeNPs were determined using EDX (Fig. 1g). Elemental analysis of PLE@FeNPs

demonstrated the presence of Fe and O in the sample, confirming the high purity of the synthesized PLE@FeNPs [50]. In the EDX analysis, it was determined that iron oxides were formed in the presence of high oxygen content.

3.2. Adsorption isotherms, adsorption kinetics, and thermodynamic analysis

The photo-Fenton process is a combination of UV radiation and produces higher amounts of hydroxyl radicals and increases the rate and extent of degradation of dye pollutants compared to the conventional Fenton mechanism [52]. Organic degradation is highly associated with OH^- formation, as OH^-·produced from H_2O_2 is the main oxidant of the photo-Fenton process [53]. In the photo-Fenton process, in addition to Fenton reactions, hydroxyl radical formation occurs with the following reactions shown in Equations (3) and (4) [54–56]. Possible dye absorption mechanism of PLE@NPs is given in Fig.S1.

$$Fe^{3+} + H_2O + \text{Sunlight} \rightarrow OH^-\bullet + Fe^{2+} + H^+ \quad (3)$$

$$H_2O_2 + \text{Sunlight} \rightarrow OH^- + OH^-.\bullet \quad (4)$$

The removal of CR using synthesized PLE@FeNPs is strongly affected by pH as pH greatly influences to the charging behavior of PLE@FeNPs. In the evaluation of dye removal studies, the effects of pH on adsorptive removal of CR by PLE@FeNPs were performed in the pH range 2–8. There was over 90% removal in all dye concentrations and pH ranges studied (except pH 2). Results of scanning performed at 25–40°C with 15 mg adsorbent and 20 ppm dye concentration in the range pH 2–8 showed the highest dye removal occurred at pH 8 (Fig. 2). In a previous study, highest dye removal activity was observed at pH 3 in studies performed with Fenton reaction as the highest production of H_2O_2 was obtained at this pH [57]. However, when the pH is above 3.5, the system is controlled by $Fe(OH)_3$ [58]. Table S1, the effectiveness at different pH values are given for Fe^{+3} (ferric) species. In our study, the highest dye removal results were obtained at pH 8. Under this condition, the removal of the pollutant is mainly due to the coagulation or sorption process, not the Fenton process. In contrast, Fe^{3+} ions control the balance [59]. A comparison of the effects of different conditions on the adsorption removal of various reactive dyes by nanoparticles is summarized in Table S1.

There was 99.9% dye removal in the presence of 15 mg PLE@FeNPs in 20 ppm dye concentration at 25°C. In addition, the dye removal rate was 99.9% at 20 ppm dye concentration for different adsorbent doses (5–20 mg) when the pH was kept constant. In another study in which CR dye removal was performed in the presence of iron oxide (Fe_2O_3) nanoparticles, the adsorbent dose was adjusted to 60 mg, and 97.9% removal was achieved in 300 minutes [60]. In our study, 99.9% dye removal was achieved in a shorter time (180 minutes) at a lower adsorbent dose (20 mg). In addition, 99.9% dye removal was achieved at 20 mg, 15 mg, and 10 mg doses in 50 ppm dye concentration, and 95.5% and 99.5% dye removal was achieved at 5 mg and 20 mg doses, respectively, with 100 ppm dye concentration, and finally, 92% dye removal was achieved at 20 mg dose in 200 ppm dye concentration. The increase in dye

concentration (10–200 mg/mL) leads to an increase in the amount of adsorbed CR per unit mass of PLE@FeNPs; therefore, with an increase in dye concentration (qe: 30.11–111.32 mg/g), more dye molecules are transferred to the adsorbent surface.

The best dye removal was achieved with a rate of 99.9% in the presence of 15 mg PLE@FeNPs at 40°C, pH 8, in 20 ppm dye concentration. The lowest dye removal rate was at pH 3, with a rate of 97%. When the pH was kept constant, dye removal was 90% at 5 mg dose of PLE@FeNPs with the initial dye concentration of 20 ppm, and 99.9% at an adsorbent dose above 5 mg. With an initial dye concentration of 50 ppm, the dye removal rate was 99.9% at 20 mg, 15 mg and 10 mg doses, and 78.5% at 5 mg dose. For an initial dye concentration of 100 ppm, the dye removal rate was 93.9% at 20 mg dose, but decreased to 81.1% at 20 mg dose in 200 ppm dye concentration. The percentage of dye removal was the highest at 20 mg PLE@FeNP adsorbent dose for 25 and 40 temperatures (Fig. 2a,b). As the amount of PLE@FeNPs increased during the reaction, the surface area increased, thus, in the active and adsorptive regions. Therefore, dye removal increases depending on the adsorbent dose increase [61].

Since CR is an anionic dye with an isoelectric point of 3.58, it is completely negatively charged at high pH. The main dye removal mechanism between pH 7–10, which we have mentioned above, is due to sorption. In this case, we consider that together with an electrostatic interaction where the positive charges of Fe^{+2} and Fe^{+3} attract the dye molecules towards the ions, porosity in the nanoparticles and the role of plant surfactants are helping to hold the dye molecules, and thereby some of them are degraded. It is possible that the adsorption by the iron nanoparticle system and the associated functional groups occurs by electrostatic attraction due to the groups that migrate over the plant to the iron nanoparticle at pH 8 (Fig. 2b).

Table 1
Comparison of degradation efficiency of various FeNPs and reactive dyes.

Plant nanoparticle	Experimental adsorption conditions	Dye	Adsorption capacity (mg/g)	Reference
GT-FeNP Green tea	*pH (No pH control)* *Initial concentration 50 mg L^{-1})* *at room temperature* *5 min. (%80 dye removed)*	Methylene blue (MB) Methylene orange (MO)	–	Shahwan et. al., 2011[62]
FONPs *P. pterocarpum*	*pH(No pH control)* *Initial concentration 50 mg L^{-1}* *220 min (90% dye removed)* *at 150 rpm* *dosage: 50 mg*	Methylene blue (MB)	–	Anchan et. Al., 2019[63]
FeNPs (*T. foenum-graecum*)	*pH (No pH control)* *Initial concentration 25.0 mg L^{-1}* *90 min (95% dye removed)* *dosage: 30 mg*	Methylene orange (MO)	–	Radini et al., 2018[64]
Iron oxide (-Fe_2O_3)	*pH(No pH control)* *Initial concentration of 100 mg L^{-1}* *At room temperature* *300 min (97.9% dye removed)* *dosage: 60 mg*	Congo red (CR)	253 mg/g	Hao et al., 2014[60]

Plant nanoparticle	Experimental adsorption conditions	Dye	Adsorption capacity (mg/g)	Reference
TW-FeNPs (Waste tea)	*pH 8.0, 25 °C* *Initial concentration of 10 mg L^{-1}* *300 min (98% dye removed)* *dosage: 0.1 g, at 100 rpm*	Phenol red (PR)	227.3 mg/g	Gautam et al., 2018[65]
FeNPs (*Datura inoxia*)	*pH 2.0* *35 °C* *Initial concentration of 10 mg L^{-1}* *75 min (98% dye removed)* *dosage: 0.1g* *at 150 rpm*	Methylene orange (MO)	81.967 mg/g	Sharma and Bhateria, 2021[61]
Iron CNPs	*pH 7.0* *25 °C* *Initial concentration of 150 µg L^{-1}* *25 min (90% dye removed)* *dosage: 0.5 g*	Congo red (CR)	43.10 (µg/g)	Ali et al., 2016[66]
PLE@FeNPs *(P. lanceolata)*	*pH 8.0* *25 °C* *Initial concentration of 50 mg L^{-1}* *180 min (99% dye removed)* *dosage: 20 mg* *at 150 rpm*	Congo red (CR)	136.79 mg/g	Present study

There are studies on isotherm and kinetic models for the removal of CR dye from wastewater with nanoparticles produced by green synthesis approaches [60, 66, 67]. When the Congo red dye removal

results using the biosorbent (PLE@FeNP) are compared in terms of correlation coefficients according to isotherm modeling, it could be concluded that the Langmuir isotherm (R^2 = 0.96 Fig. 3a) is the best among the mean values of R^2, followed by the Freundlich isotherm (R^2 = 0.95 Fig. 3b, Table S2). The Langmuir model assumes that CR adsorption on PLE@FeNPs occurs predominantly as a monolayer with a homogeneous dye molecule distribution on the surface; all adsorbed substances have the same adsorption energy and do not move on the solid surface. On the other hand, Freundlich isotherm is an experimental model used to describe multilayered adsorption. This model assumes that possible interactions occur between adsorbed groups in heterogeneous surface regions with different energies. In addition, the Langmuir separation factor (R_L value) indicates the shape of the isotherm. In current study, R_L was determined to be 0.17 (Table S2). According to Mckay (1982)[68], R_L values between 0 and 1 indicate appropriate absorption; that is, the process is favorable. The high values of K_F and n in the Freundlich isotherm indicates easy separation of iron nanoparticles from wastewater and high adsorption capacity. The fact that the n value, which is related to the distribution of ions bound to the adsorbent surface, is positive for the adsorption of the nanoparticle indicates that the adsorption is favorable (Table S2).

Kinetic analyses were performed to obtain the rate of biosorption, which determines the contact time required for biosorption of CR with iron nanoparticles. Kinetic analyses were examined according to the pseudo-first-order (Fig. 3d) and pseudo-second-order models (Fig. 3e). The biosorption kinetics of the dye material used in our study was observed to be more compatible with the pseudo-second-order kinetic model (R^2 = 0.99, Fig. 3d) at 25°C. When the model that best represents the adsorption kinetics is the pseudo-second-order kinetic model, the step that controls the rate of the adsorption process is the adhesion to the adsorbent surface. In addition, the estimated maximum adsorption capacity for CR adsorption in the current study ($q_{e\ cal}$ = 79.11; q_e exp = 77.10 mg/g) was slightly higher than the experimental maximum adsorption capacity (Table S2).

Thermodynamic analyses determine the nature of the adsorption process (exothermic/endothermic). They help to distinguish the chemical and physical reactions during adsorption [69]. Evaluations of the thermodynamics showed that the reaction occurs spontaneously (ΔG -26.6 kJ mol^{-1}), and it is exothermic (ΔH -35.3 kJ mol^{-1}); the results are given in Fig. 3f and Table 2. A value of ΔH° < 0 indicates that this process is exothermic and low temperatures are in favor of adsorption, while negative ΔG° values indicate that adsorption occurs spontaneously [70, 71].

Table 2
Thermodynamic parameters of CR adsorption onto the PLE@FeNPs.

Adsorbent	Temp (K/°C)	K_L	ΔG^o (KJ mol^{-1})	ΔH^o (KJ mol^{-1})	ΔS^o (KJ^{-1} mol^{-1})	R^2
PLE@FeNPs	298/25	10.765	-26.671	-35.3422	-98.8414	1.000
	313/40	5.435	-14.140			

3.3. Cell Proliferation Analysis

The cytotoxic effects of PLE@FeNPs and *P. lanceolata* extract at different concentrations were studied against A549 and SH-SY5Y cell lines (Fig. 4a, 4b, respectively). PLE@FeNPs and *P. lanceolata* extracts reduced cell viability 71.8% and 65.6%, respectively in A549 cancer cell line at 500 µg/mL concentration, and 84.4% and 82%, respectively, at 1000 µg/mL concentration. The viability of A549 cancer cells decreased with an increasing concentration. The concentration and size of nanoparticles play an important role in inducing toxicity. Nanoparticles interact with NADPH oxidases in the cell membrane and mitochondria to form superoxide anions. This causes cytotoxicity by activating redox reactions [51, 72]3 While *P. lanceolata* extract showed 83.3% and 73.8% neurotoxicity against SH-SY5Y cell line at 1000 µg/mL and 500 µg/mL concentrations, respectively, the neurotoxic effect was lower at other concentrations tested. In the neurotoxicity tests performed on human nerve cells, PLE@FeNPs did not show any neurotoxic activity against the SH-SY5Y cell line at concentrations of 1000 µg/mL and 500 µg/mL suggesting PLE@FeNPs were not toxic to SH-SY5Y cells. The reason why they do not show neurotoxic activity, especially at concentrations of 1000 µg/mL and 500 µg/mL, is considered to be due to the antioxidant activity of iron and organic active compounds in nanoparticles. Nanoparticles can be transmitted to the blood system through the digestive system in the body and then reach the liver, brain, and other organs. Therapeutic drugs can be administered to the brain and other organs through nanoparticles [73]. There was no study investigating the effect of PLE@FNPs on neuroblastoma cell line in the literature. The lack of significant cell toxicity [74] in a different study examining the neurotoxicity effect of MgO nanoparticles on the SH-SY5Y cell line coincides with the results of our study.

3.4. DNA fragmentation assay

The DNA fragmentation assay was carried out to examine the impacts of PLE@FeNPs on A549 cells. The results of our study demonstrated that PLE@FeNPs cleaved nuclear DNA of human A549 cells by forming ladder pattern as illustrated in Fig. 4c. The control cells (MRC5) have not shown any fragmented DNA.

3.5. Antioxidant activity and total phenolic and flavonoid content

Total DPPH radical scavenging, metal chelation and total antioxidant of the water extract obtained from *P. lanceolata* are given in Fig. 5a and 5b, respectively. DPPH removal activity of *P. lanceolata* plant extract was calculated as 78.86 ± 0.65%, and DPPH removal activity of PLE@FeNPs was calculated as 89.79 ± 0.21%. DPPH removal activity of PLE@FeNPs > *P. lanceolata* > BHA, respectively. Phenolic and flavonoid compounds are strong radical scavengers and have high reducing power [75]. Thus, the high rate of DPPH radical scavenging of *P. lanceolata* can be attributed to the presence of these compounds in the extract. PLE@FeNPs also achieved a high rate of radical removal. This could be interpreted as the fact that 983, 1578, and 1726 cm^{-1} peaks in the FTIR spectrum of PLE@FeNPs originate from C = C ring polyphenol (Fig. 2b). Organic groups on the surface of nanoparticles were effective in radical removal. Many studies have shown that iron nanoparticles have a high DPPH radical scavenging activity [76, 77].

The total antioxidant activity of the water extract of *P. lanceolata* and PLE@FeNPs was 31290.91 ± 190.07 and 3624.24 ± 150.04 µg α-tocopherol/g, respectively (Fig. 5c). The total antioxidant activity of P. lanceolata plant extract was higher than that of PLE@FeNPs. PLE@FeNPs showed strong metal chelating potential compared to EDTA as a reference. This arises from the synergy between iron metals and functional groups. The metal chelating activity of the P. lanceolata plant extract was calculated as 13.52 ± 0.97%, and for PLE@FeNPs at 74.39 ± 0.78%. The ranking for metal chelating activity was EDTA > PLE@FeNPs > P. lanceolata, respectively. Bahadori et al. (2020)[75] reported that the best iron chelation was in the water extract (95%) in their study, where they calculated the metal chelating activity of different fractions of P. lanceolata. The total phenolic and total flavonoid contents of the water extract obtained from P. lanceolata are given in Fig. 5d and 5e, respectively. The total phenolic content of P. lanceolata water extract and PLE@FeNPs was calculated as 47.32 ± 1.90 and 7.35 ± 0.85 mg GAE/g, respectively, and total flavonoid content was 7.47 ± 0.89 and 4.89 ± 0.50 mg QE/g, respectively. PLE@FeNPs were observed to have a lower phenolic and flavonoid content than the P. lanceolata plant extract. The phenolic and flavonoid contents found in the plant extract are in agreement with previous studies [78]. Beara et al. (2009)[79]reported phenolic contents ranging from 38 to 70 mg GAE/g and flavonoid content ranging from 6 to 12 mg QE/g for five different Plantago species. Since phenolic and flavonoid compounds have functional properties and an important role in the green synthesis of nanoparticles, it may be useful to determine their contents. The presence of phenolic and flavonoid compounds may correspond to the extracts used in the biosynthesis of nanoparticles [80].

3.6 Antimicrobial activity

Minimum inhibition concentration (MIC) values of *P. lanceolata* L. plant extract and PLE@FeNPs are shown in Table 3. MIC values for microorganisms tested with *P. lanceolata* extract are as follows: *K. pneumoniae* EMCS, 0.3125 mg/mL; *E. coli ATCC*® 25922™, 5 mg/mL; *S. cerevisiae* and *S. aureus ATCC*® *29213*™, 0.625 mg/mL (Fig. S3). In studies which determined the MIC value of *P. lanceolata* extract on gram-positive *Streptococcus* species, the MIC values for *P. lanceolata* extract were obtained at concentrations of 0.5–1 mg/l, although their sensitivity varied significantly [81]. On the other hand, in the study of Sharifa et al. (2008)[82], which determined the effectiveness of *P. major* extracts in gram-positive and negative bacteria, the researchers reported that the *P. major* extract caused significant changes in the cell wall structure of gram-positive bacteria, whereas its effectiveness was low in gram-negative bacteria. In our study, the most resistant strain was determined to be gram-negative *E. coli* with a concentration of 5 mg/mL. The MIC values for microorganisms tested with PLE@FeNPs was 0.625 (mg/mL) for *K. pneumoniae* EMCS, *E. coli ATCC*® 25922™, and *S cerevisiae;* it was 0.3125 (mg/mL) for *S. aureus ATCC*® *29213*™. In this study, it is clear that the nanoparticle's high antioxidant activity contributes to a better antimicrobial profile. This contribution may be related to the content of phenolic compounds as well as the presence of iron in the nanoparticle. Some other studies reported that nanoparticle concentration has a significant effect on the inactivation of microorganisms [83, 84]. It has been suggested in the literature that nanoparticles slow the mechanism of antimicrobial activity in two ways. The first mechanism of action is disturbances in the cell structure by the accumulation of nanoparticles in the cytoplasm, and the second mechanism of action is the interaction of the nanoparticles with oxygen radicals by passing into

the cell after binding to the cell wall, subsequently creating oxidative stress [85]. The most important mechanism of action of antibiotics on microorganisms is that they kill microorganisms as a result of damage to DNA, protein and cell membrane [86]. On the other hand, nanoparticles of 10–80 nm size penetrate the cell wall surface and interact with the oxygen inside the cell, causing oxidative stress. As a result, microorganisms are killed [87]. According to the results of the TEM analysis, the interaction of nanoparticles of 8 nm average size with the cell wall and the oxygen inside the cell showed a high efficiency on the oxidative stress of microorganisms. While iron oxide nanoparticles obtained by green synthesis from *Carica papaya* showed moderate antibacterial activity against bacterial strains of *Klebsiella spp., E. coli, Pseudomonas spp.*, and *S. aureus* at 50 mg/mL [88], in the present study, an effective antimicrobial activity was observed at very low concentrations (0.3125 mg/mL) (Table 3 and Fig. S3). Analyses of the antibacterial properties of PLE@FeNPs showed that the greatest effect was observed in *S. aureus* compared to other microorganisms. Vitta et al. (2020) [80] attributed the antimicrobial activity they obtained against similar microorganisms to the small size of the nanoparticles.

Table 3
Minimum inhibitory concentration (MIC) values for antimicrobial activity.

	Microorganism	PLE@FeNP (MIC)	*P. lanceolata* (MIC)
A	*Klebsiella pneumoniae;* EMCS	0,625 (mg/mL)	0,3125 (mg/mL)
B	*Escherichia coli*; *ATCC*® 25922™	0,625 (mg/mL)	5 (mg/mL)
C	*Saccharomyces cerevisiae ATCC*® 76521™	0,625 (mg/mL)	0,625 (mg/mL)
D	*Staphylococcus aureus*; *ATCC*® 29213™	0,3125 (mg/mL)	0,625 (mg/mL)

4. Conclusion

The aim of the current study was the green synthesis, characterisation and Congo Red (CR) dye removal, cytotoxic, antioxidant and antimicrobial properties of PLE@FeNPs. The morphology and physical properties of PLE@FeNPs were characterized by FTIR, XRD, SEM, EDX, TEM and DLS analysis. The synthesis of PLE@FeNPs using *P. lanceolata* L. plant extract with the green synthesis method is offered as an alternative to traditional methods, considering the advantages such as low cost, non-toxicity, environmental friendliness, and abundance of iron and the *P. lanceolata* plant. The optimum adsorption conditions of pH, temperature and adsorbent amount for CR removal were found as pH 4, 25 ℃ and 15 mg respectively. The CR removal using PLE@FeNPs reached a very high removal efficiency of 99%. PLE@FeNPs showed bactericidal and antioxidant activities. The cytotoxicity experiments demonstrtaed that PLE@FeNPs possessed significant cytotoxic effects in human lung cancer (A549) cell line while no such effects were observed on human neuroblastoma (SH-SY5Y) cell line. PLE@FeNPs were also shown to cause DNA fragmentation on A549 cells. Overall these results revealed further applications of PLE@FeNPs in CR dye removal and biological applications.

References

1. A.A. Gadgeel, S.T. Mhaske, C. Duerr et al., In-Situ Preparation and haracterization of Aconitic Acid Capped Fe3O4 Nanoparticle by Using Citric Acid as a Reducing Agent. J. Inorg. Organomet. Polym. **29**, 1688–1700 (2019). https://doi.org/10.1007/s10904-019-01131-1
2. O.P. Bolade, A.B. Williams, N.U. Benson, Green synthesis of iron-based nanomaterials for environmental remediation: A review. Environ Nanatechnol. Monit Manag **13**, 100279 (2020). https://doi.org/10.1016/J.ENMM.2019.100279
3. K. Pakzad, H. Alinezhad, M. Nasrollahzadeh, Green synthesis of Ni@Fe_3O_4 and CuO nanoparticles using *Euphorbia maculata* extract as photocatalysts for the degradation of organic pollutants under UV-irradiation. Ceram. Int. **45**, 17173–17182 (2019). https://doi.org/10.1016/j.ceramint.2019.05.272
4. S.S. Salem, A. Fouda, Green Synthesis of Metallic Nanoparticles and Their Prospective Biotechnological Applications: an Overview. Biol. Trace Elem. Res. **199**, 344–370 (2011). https://doi.org/10.1007/s12011-020-02138-3/Published
5. T.P. Chau, G.R. Veeraragavan, M. Narayanan, A. Chinnathambi, S.A. Alharbi, B. Subramani, K. Brindhadevi, T. Pimpimon, S. Pikulkaew, Green synthesis of Zirconium nanoparticles using *Punica granatum* (pomegranate) peel extract and their antimicrobial and antioxidant potency. Environ. Res. **209**, 112771 (2022). https://doi.org/10.1016/j.envres.2022.112771
6. Y. Huo, Y.X. Han, P. Singh, P. Jong, ·, Kang, · Jian, Y. Pu, Chun, ·, H. Piao, C. Deok, ·, Yang, 2021. Antimicrobial, antioxidant, and anticancer potentials of AgCl nanoparticles biosynthesized by *Flavobacterium panacis*. Appl. Phys. A. 127, 227 (2021). https://doi.org/10.1007/s00339-021-04386-z
7. Nayantara, P. Kaur, Biosynthesis of nanoparticles using eco-friendly factories and their role in plant pathogenicity: a review. Biotechnol. Res. Innov. **2**, 63–73 (2018). https://doi.org/10.1016/j.biori.2018.09.003
8. S. Das, A. Pandey, S. Pal, H. Kolya, T. Tripathy, Green synthesis, characterization and antibacterial activity of gold nanoparticles using hydroxyethyl starch-g-poly (methylacrylate-co-sodium acrylate): A novel biodegradable graft copolymer. J. Mol. Liq **212**, 259–265 (2015). https://doi.org/10.1016/j.molliq.2015.09.020
9. P. Cheviron, F. Gouanvé, E. Espuche, Green synthesis of colloid silver nanoparticles and resulting biodegradable starch/silver nanocomposites. Carbohydr. Polym. **108**, 291–298 (2014). https://doi.org/10.1016/j.carbpol.2014.02.059
10. L. Katata-Seru, T. Moremedi, O.S. Aremu, I. Bahadur, Green synthesis of iron nanoparticles using *Moringa oleifera* extracts and their applications: removal of nitrate from water and antibacterial activity against *Escherichia coli*. J. Mol. Liq **256**, 296–304 (2018). https://doi.org/10.1016/j.molliq.2017.11.093
11. R.G. Suthar, B. Gao, Nanotechnology for drinking water purification, Water Purif. Acad. Press. 2017, 75–118, https://doi.org/10.1016/B978-0-12-804300-4.00003-4

12. A.C. de Lima Barizão, M.F. Silva, M. Andrade, F.C. Brito, R.G. Gomes, R. Bergamasco, Green synthesis of iron oxide nanoparticles for tartrazine and bordeaux red dye removal. J. Environ. Chem. Eng. **8**(1), 103618 (2020). https://doi.org/10.1016/j.jece.2019.103618
13. G.Z. Kyzas, N.K. Lazaridis, A.C. Mitropoulos, Removal of dyes from aqueous solutions with untreated coffee residues as potential low-cost adsorbents: Equilibrium, reuse and thermodynamic approach. Chem. Eng. Technol. **189**, 148–159 (2012). https://doi.org/10.1016/j.cej.2012.02.045
14. S. Joshi, V.K. Garg, N. Kataria, K. Kadirvelu, Applications of Fe_3O_4@ AC nanoparticles for dye removal from simulated wastewater. Chemosphere **236**, 124280 (2019). https://doi.org/10.1016/j.chemosphere.2019.07.011
15. T. Sh Atabaev, 2017. PEG-Coated Superparamagnetic Dysprosium-Doped Fe_3O_4 Nanoparticles for Potential MRI Imaging. https://doi.org/10.1007/s12668-017-0447-6
16. D.L. Fedlheim, C.A. Foss, *Metal Nanoparticles: Synthesis, Characterization, and Applications*, 1st edn. (CRC Press, 2001), https://doi.org/10.1201/9780367800475
17. A. Rajendran, M. Alsawalha, T. Alomayri, Biogenic synthesis of husked rice-shaped iron oxide nanoparticles using coconut pulp (*Cocos nucifera* L.) extract for photocatalytic degradation of Rhodamine B dye and their in vitro antibacterial and anticancer activity. J. Saudi Chem. Soc. **25**, 101307 (2021). https://doi.org/10.1016/j.jscs.2021.101307
18. J. Xu et al., Decorated of Au NPs over L-arginine-modified Fe_3O_4 nanoparticles as a novel nanomagnetic composite for the treatment of human ovarian cancer. Arab. J. Chem. **14**(8), 103283 (2021). https://doi.org/10.1016/j.arabjc.2021.103283
19. S. Abdolmohammadi, Z. Hossaini, M.R. Poor Heravi, PANI-Fe3O4@ZnO nanocomposite as magnetically recoverable organometallic nanocatalyst promoted synthesis of new Azo chromene dyes and evaluation of their antioxidant and antimicrobial activities. Mol. Divers. (2021). https://doi.org/10.1007/s11030-021-10309-0
20. S.A. Mousa, El-Sayed, R. El-Sayed, S.S. Mohamed, M.A. Abo El-Seoud, A.A. Elmehlawy, D.A.M. Abdou, n.d. Novel mycosynthesis of Co_3O_4, CuO, Fe_3O_4, NiO, and ZnO nanoparticles by the endophytic Aspergillus terreus and evaluation of their antioxidant and antimicrobial activities. Appl. Microbiol. Biotechnol. **105**, 741–753 (2021). https://doi.org/10.1007/s00253-020-11046-4
21. S.F. Mousavi, Z. Hossaini, F. Rostami-Charati, N. Nami, Synthesis of Benzochromene Derivatives Using Reusable Fe_3O_4 /ZnO Magnetic Nanoparticles: Study of Antioxidant and Antibacterial Activity Polycycl. Aromat. Compd. (2021). https://doi.org/10.1080/10406638.2021.1991390
22. S. Shams, A.U. Khan, Q. Yuan, W. Ahmad, Y. Wei, Z.U.H. Khan, A. Shams, Sumaira, Ahmad, A.U. Rahman, S. Ullah, Facile and eco-benign synthesis of Au@Fe_2O_3 nanocomposite: Efficient photocatalytic, antibacterial and antioxidant agent. J. Photochem. Photobiol B Biol. **199**, 111632 (2019). https://doi.org/10.1016/j.jphotobiol.2019.111632
23. N.U.M. Nizam, M.M. Hanafiah, E. Mahmoudi et al., The removal of anionic and cationic dyes from an aqueous solution using biomass-based activated carbon. Sci. Rep. **11**, 8623 (2021). https://doi.org/10.1038/s41598-021-88084-z

24. C.V. Reddy, I.N. Reddy, V.V.N. Harish, K.R. Reddy, N.P. Shetti, J. Shim, T.M. Aminabhavi, Efficient removal of toxic organic dyes and photoelectrochemical properties of iron-doped zirconia nanoparticles. Chemosphere **239**, 124766 (2020). https://doi.org/10.1016/j.chemosphere.2019.124766
25. Y. Yi, G. Tu, P.E. Tsang, S. Xiao, Z. Fang, Green synthesis of iron-based nanoparticles from extracts of *Nephrolepis auriculata* and applications for Cr (VI) removal. Mater. Lett. **234**, 388–391 (2019). https://doi.org/10.1016/j.matlet.2018.09.137
26. U.S. Harput, Y. Genc, I. Saracoglu, Cytotoxic and antioxidative activities of *Plantago lagopus* L. and characterization of its bioactive compounds. Food Chem. Toxicol. **50**(5), 1554–1559 (2012). https://doi.org/10.1016/j.fct.2012.01.019
27. Z. Nizioł-Łukaszewska, K. Gaweł Bęben, K. Rybczyńska Tkaczyk, A. Jakubczyk, M. Karaś, T. Bujak, Biochemical properties, UV-protecting and fibroblast growth-stimulating activity of *Plantago lanceolata* L. extracts. Ind. Crops Prod. **138**, 111453 (2019). https://doi.org/10.1016/j.indcrop.2019.06.016
28. E.C. Dreaden, A.M. Alkilany, X. Huang, C.J. Murphy, M.A. El-Sayed, The golden age: gold nanoparticles for biomedicine. Chem. Soc. Rev. **41**(7), 2740–2779 (2012)
29. S.Y. Lagergren, Zur theorie der sogenannten adsorption geloster stoffe K. Vet. Akad. Handl. **24**(4), 1–39 (1898)
30. Y.S. Ho, G. McKay, Pseudo-second order model for sorption processes. Process. Biochem. **34**(5), 451–465 (1999). https://doi.org/10.1016/S0032-9592(98)00112-5
31. M. Hajji, R. Jarraya, I. Lassoued, O. Masmoudi, M. Damak, M. Nasri, GC/MS and LC/MS analysis, and antioxidant and antimicrobial activities of various solvent extracts from *Mirabilis jalapa* tubers. Process. Biochem. **45**(9), 1486–1493 (2010). https://doi.org/10.1016/j.procbio.2010.05.027
32. L. Estevinho, A.P. Pereira, L. Moreira, L.G. Dias, E. Pereira, Antioxidant and antimicrobial effects of phenolic compounds extracts of Northeast Portugal honey. Food Chem. Toxicol. **46**(12), 3774–3779 (2008). https://doi.org/10.1016/j.fct.2008.09.062
33. T.C. Dinis, V.M. Madeira, L.M. Almeida, Action of phenolic derivatives (acetaminophen, salicylate, and 5-aminosalicylate) as inhibitors of membrane lipid peroxidation and as peroxyl radical scavengers. Arch. Biochem. Biophys. **315**(1), 161–169 (1994). https://doi.org/10.1006/abbi.1994.1485
34. T. Hatano, H. Kagawa, T. Yasuhara, T. Okuda, Two new flavonoids and other constituents in licorice root: their relative astringency and radical scavenging effects. Chem. Pharm. Bull. **36**(6), 2090–2097 (1988). https://doi.org/10.1248/cpb.36.2090
35. Y. Wenli, Z. Yaping, S. Bo, The radical scavenging activities of *Radix puerariae* isoflavonoids: A chemiluminescence study. Food Chem. **86**(4), 525–529 (2004). https://doi.org/10.1016/j.foodchem.2003.09.005
36. M. Tartik, E. Darendelioglu, G. Aykutoglu, G. Baydas, Turkish propolis supresses MCF-7 cell death induced by homocysteine. Biomed. Pharmacother **82**, 704–712 (2016). https://doi.org/10.1016/j.biopha.2016.06.013

37. J. Gierschner, J.L. Duroux, P. Trouillas, UV/Visible spectra of natural polyphenols: A time-dependent density functional theory study. Food Chem. **131**(1), 79–89 (2012). https://doi.org/10.1016/j.foodchem.2011.08.034
38. H. Veisi, A. Rashtiani, V. Barjasteh, Biosynthesis of palladium nanoparticles using *Rosa canina* fruit extract and their use as a heterogeneous and recyclable catalyst for Suzuki-Miyaura coupling reactions in water. Appl. Organomet. Chem. **30**(4), 231–235 (2016). https://doi.org/10.1002/aoc.3421
39. J.A.A. Abdullah, L.S. Eddine, B. Abderrhmane, M. Alonso González, A. Guerrero, A. Romero, Green synthesis and characterization of iron oxide nanoparticles by *Pheonix dactylifera* leaf extract and evaluation of their antioxidant activity. Sustain. Chem. Pharm. **17**, 100280 (2020). https://doi.org/10.1016/j.scp.2020.100280
40. T. Wang, X. Jin, Z. Chen, M. Megharaj, R. Naidu, Green synthesis of Fe nanoparticles using eucalyptus leaf extracts for treatment of eutrophic wastewater. Sci. Total Environ. **466**, 210–213 (2014). https://doi.org/10.1016/j.scitotenv.2013.07.022
41. M. Sulpizi, M.P. Gaigeot, M.J. Sprik, The silica-water interface: how the silanols determine the surface acidity and modulate the water properties. J. Chem. Theory Comput. **8**(3), 1037–1047 (2012). https://doi.org/10.1021/ct2007154
42. R. Jain, S. Mendiratta, L. Kumar, A. Srivastava, Green synthesis of iron nanoparticles using *Artocarpus heterophyllus* peel extract and their application as a heterogeneous Fenton-like catalyst for the degradation of Fuchsin Basic dye. Curr. Opin. Green. Sustain. Chem. **4**, 100086 (2021). https://doi.org/10.1016/j.crgsc.2021.100086
43. K.M. Kumar, B.K. Mandal, K.S. Kumar, P.S. Reddy, B. Sreedhar, Biobased green method to synthesise palladium and iron nanoparticles using *Terminalia chebula* aqueous extract. Spectrochim. Acta A Mol. Biomol. Spectrosc. **102**, 128–133 (2013). https://doi.org/10.1016/j.saa.2012.10.015
44. Q. Lan, C. Liu, F. Yang, S. Liu, J. Xu, D. Sun, Synthesis of bilayer oleic acidcoated Fe_3O_4 nanoparticles and their application in pH-responsive Pickering emulsions. Chem. Eng. Technol. **310**(1), 260–269 (2007). https://doi.org/10.1016/j.jcis.2007.01.081
45. K. Palanisamy, V. Devabharathi, N.M. Sundaram, The utility of magnetic iron oxide nanoparticles stabilized by carrier oils in removal of heavy metals from waste water. IJRANSS. **1**(4), 15–22 (2013)
46. R.K. Gautam, V. Rawat, S. Banerjee, M.A. Sanroman, S. Soni, S.K. Singh, M.C. Chattopadhyaya, Synthesis of bimetallic Fe–Zn nanoparticles and its application towards adsorptive removal of carcinogenic dye malachite green and Congo red in water. J. Mol. Liq **212**, 227–236 (2015). https://doi.org/10.1016/j.molliq.2015.09.006
47. A. Mukherjee, D. Dutta, S. Banerjee, E. Ringø, E. Breines, M. Hareide, E. Chandra, G. Ghosh, K., Potential probiotics from Indian major carp, *Cirrhinus mrigala* Characterization, pathogen inhibitory activity, partial characterization of bacteriocin and production of exoenzymes. Vet. Sci. Res. **108**, 76–84 (2016). https://doi.org/10.1016/j.rvsc.2016.08.011

48. S. Duman, B. Kaya, F. Caf, B. Enez, S.A. Fincan, Innovative hydrogen release from sodium borohydride hydrolysis using biocatalyst-like Fe_2O_3 nanoparticles impregnated on *Bacillus simplex* bacteria. Int. J. Hydrog **46**(29), 15410–15430 (2021). https://doi.org/10.1016/j.ijhydene.2021.02.028
49. S. Bhattacharjee, DLS and zeta potential-what they are and what they are not? J. Control Release **235**, 337–351 (2016). https://doi.org/10.1016/j.jconrel.2016.06.017
50. K. Singh, D.S. Chopra, D. Singh, N. Singh, Optimization and ecofriendly synthesis of iron oxide nanoparticles as potential antioxidant. Arab. J. Chem. **13**(12), 9034–9046 (2020). https://doi.org/10.1016/j.arabjc.2020.10.025
51. J. Yoonus, R. Resmi, B. Beena, Evaluation of antibacterial and anticancer activity of green synthesized iron oxide (α-Fe_2O_3) nanoparticles. Mater. Today: Proc. 46(8), 2969–2974 (2021). https://doi.org/10.1016/j.matpr.2020.12.426
52. M. Ahmadi, M. Mohseni, F. Vahabzadeh, Study on trend of biodegradability of phenolic compounds during photo-Fenton advanced oxidation process. Iran. J Chem Eng **5**(4), 23–32 (2008). https://doi.org/10.1039/C4RA16959J
53. Y.W. Kang, K.Y. Hwang, Effects of reaction conditions on the oxidation efficiency in the Fenton process. Water Res. **34**(10), 2786–2790 (2000). https://doi.org/10.1016/S0043-1354(99)00388-7
54. M. Tamimi, S. Qourzal, N. Barka, A. Assabbane, Y. Ait-Ichou, Methomyl degradation in aqueous solutions by Fenton's reagent and the photo-Fenton system. Sep. Purif. Technol. **61**(1), 103–108 (2008). https://doi.org/10.1016/j.seppur.2007.09.017
55. M. Muruganandham, M. Swaminathan, Decolourisation of Reactive Orange 4 by Fenton and Photo-Fenton Oxidation Technology. Dyes Pigm. **63**, 315–321 (2004). https://doi.org/10.1016/j.dyepig.2004.03.004
56. I.B. Will, J.E. Moraes, A.C. Teixeira, R. Guardani, C.A. Nascimento, Photo-Fenton degradation of wastewater containing organic compounds in solar reactors. Sep. Purif. Technol. **34**(1–3), 51–57 (2004). https://doi.org/10.1016/S1383-5866(03)00174-6
57. F. Fu, Q. Wang, B. Tang, Effective degradation of CI Acid Red 73 by advanced Fenton process. J. Hazard. Mater. **174**(1–3), 17–22 (2010). https://doi.org/10.1016/j.jhazmat.2009.09.00943
58. M. Zhou, Q. Yu, L. Lei, G. Barton, Electro-Fenton method for the removal of methyl red in an efficient electrochemical system. Sep. Purif. Technol. **57**(2), 380–387 (2007). https://doi.org/10.1016/j.seppur.2007.04.021
59. P.V. Nidheesh, R. Gandhimathi, S.T. Ramesh, Degradation of dyes from aqueous solution by Fenton processes: a review. Environ. Sci. Pollut Res. **20**(4), 2099–2132 (2013). https://doi.org/10.1007/s11356-012-1385-z
60. T. Hao, C. Yang, X. Rao, J. Wang, C. Niu, X. Su, Facile additive-free synthesis of iron oxide nanoparticles for efficient adsorptive removal of Congo red and Cr (VI). Appl. Surf. Sci. **292**, 174–180 (2014). https://doi.org/10.1016/j.apsusc.2013.11.108
61. Y. Sharma, Bhateriar, Phytoproduction of ıron nanoparticles for methyl orange removal and its optimization studies. Plant. Arch. **21**(1), 939–954 (2021).

https://doi.org/10.51470/plantarchives.2021.v21.no1.130

62. T. Shahwan, S.A. Sirriah, M. Nairat, E. Boyacı, A.E. Eroğlu, T.B. Scott, K.R. Hallam, Green synthesis of iron nanoparticles and their application as a Fenton-like catalyst for the degradation of aqueous cationic and anionic dyes. Chem. Eng. J. **172**(1), 258–266 (2011). https://doi.org/10.1016/j.cej.2011.05.103
63. S. Anchan, S. Pai, H. Sridevi, T. Varadavenkatesan, R. Vinayagam, R. Selvaraj, Biogenic synthesis of ferric oxide nanoparticles using theleaf extract of *Peltophorum pterocarpum* and their catalytic dye degradation potential. Biocatal. Agric. **20**, 101251 (2019). https://doi.org/10.1016/j.bcab.2019.101251
64. I.A. Radini, H. Hasan, M.A. Malik, Z. Khan, Biosynthesis of iron nanoparticles using Trigonella foenum-graecum seed extract for photocatalytic methyl orange dye degradation and antibacterial applications. J. Photochem. Photobiol B Biol. **183**, 154–163 (2018). https://doi.org/10.1016/j.jphotobiol.2018.04.014
65. A. Gautam, S. Rawat, L. Verma, J. Singh, S. Sikarwar, B. Yadav, A.S. Kalamdhad, 2018. Green synthesis of iron nanoparticle from extract of waste tea: An application for phenol red removal from aqueous solution. Environ. Nanotechnol. Monit. Manag. 10, 377–387(2018). https://doi.org/10.1016/j.enmm.2018.08.003
66. I. Ali, Z.A. Al-Othman, A. Alwarthan, Molecular uptake of congo red dye from water on iron composite nano particles. J. Mol. Liq 224(Part A), 171–176 (2016). https://doi.org/10.1016/j.molliq.2016.09.108
67. C.M. Simonescu, A. Tătăruş, D.C. Culiţă, N. Stănică, I.A. Ionescu, B. Butoi, A.M. Banici, Comparative study of CoFe2O4 nanoparticles and CoFe2O4-chitosan composite for Congo Red and Methyl Orange removal by adsorption. Nanomaterials **11**(3), 711 (2021). https://doi.org/10.3390/nano11030711
68. G. McKay, Adsorption of dyestuffs from aqueous solutions with activated carbon I: Equilibrium and batch contact-time studies. J. Chem. Technol. Biotechnol. **32**, 759–772 (1982). https://doi.org/10.1002/jctb.5030320712
69. R.L. Tseng, K.T. Wu, F.C. Wu, R.S. Juang, Kinetic studies on the adsorption of phenol, 4- chlorophenol, and 2, 4-dichlorophenol from water using activated carbons. J. Environ. Manage. **91**(11), 2208–2214 (2010). https://doi.org/10.1016/j.jenvman.2010.05.018
70. T. Liu, W. Sun, X. Sun, H. Ai, Thermodynamic analysis of the effect of the hierarchical architecture of a superhydrophobic surface on a condensed drop state. Langmuir. **26**(18), 14835–14841 (2010). https://doi.org/10.1021/la101845t
71. A. Demirbas, A. Sari, O. Isildak, Adsorption thermodynamics of stearic acid onto bentonite. J. Hazard. Mater. **135**(1–3), 226–231 (2006). https://doi.org/10.1016/j.jhazmat.2005.11.056
72. M. Radu, M.C. Munteanu, S. Petrache, A.I. Serban, D. Dinu, A. Hermenean, C. Sima, A. Dinischiotu, Depletion of intracellular glutathione and increased lipid peroxidation mediate cytotoxicity of

hematite nanoparticles in MRC-5 cells. Acta Biochim. Pol. **57**(3), 355–360 (2010). https://doi.org/10.18388/abp.2010_2416

73. M. Abudayyak, E. Guzel, G. Özhan, 2017. Nickel oxide nanoparticles are highly toxic to SH-SY5Y neuronal cells. Neurochem. Int. 108, 7–14 (2017). https://doi.org/10.1016/j.neuint.2017.01.017
74. O.B. Nalci, H. Nadaroglu, S. Genc, A. Hacımuftuoglu, A. Alaylı, The effects of MgS nanoparticles-Cisplatin-bioconjugate on SH-SY5Y neuroblastoma cell line. Mol. Biol. Rep. **47**, 9715–9723 (2020). https://doi.org/10.1007/s11033-020-05987-2
75. M.B. Bahadori, C. Sarikurkcu, M.S. Kocak, M. Calapoglu, M.C. Uren, O. Ceylan, *Plantago lanceolata* as a source of health-beneficial phytochemicals: Phenolics profile and antioxidant capacity. Food Biosci. **34**, 100536 (2020). https://doi.org/10.1016/j.fbio.2020.100536
76. M. Khatami, H.Q. Alijani, B. Fakheri, M.M. Mobasseri, M. Heydarpour, Z.K. Farahani, A.U. Khan, Super-paramagnetic iron oxide nanoparticles (SPIONs): Greener synthesis using Stevia plant and evaluation of its antioxidant properties. J. Clean. Prod. **208**, 1171–1177 (2019). https://doi.org/10.1016/j.jclepro.2018.10.182
77. R. Periakaruppan, X. Chen, K. Thangaraj, A. Jeyaraj, H.H. Nguyen, Y. Yu, S. Hu, L. Lu, X. Li, Utilization of tea resources with the production of superparamagnetic biogenic iron oxide nanoparticles and an assessment of their antioxidant activities. J. Clean. Prod. **278**, 123962 (2021). https://doi.org/10.1016/j.jclepro.2020.123962
78. A. Dalar, M. Türker, I. Konczak, Antioxidant capacity and phenolic constituents of *Malva neglecta* Wallr. and *Plantago lanceolata* L. from Eastern Anatolia Region of Turkey. J. Herb. Med. 2(2), 42–51 (2012). https://doi.org/10.1016/j.hermed.2012.03.001
79. I.N. Beara, M.M. Lesjak, E.D. Jovin, K.J. Balog, G.T. Anačkov, D.Z. Orčić, N.M. Mimica-Dukić, Plantain (Plantago L.) species as novel sources of flavonoid antioxidants. J. Agric. Food Chem. **57**(19), 9268–9273 (2009). https://doi.org/10.1021/jf902205m
80. Y. Vitta, M. Figueroa, M. Calderon, C. Ciangherotti, Synthesis of iron nanoparticles from aqueous extract of *Eucalyptus robusta* Sm and evaluation of antioxidant and antimicrobial activity. Mater. Sci. Eng. Technol. **3**, 97–103 (2020). https://doi.org/10.1016/j.mset.2019.10.014
81. G.F. Ferrazzano, T. Cantile, L. Roberto, A. Ingenito, M. Catania, R. Roscetto, E. Palumbo, G. Zarrelli, A. Pollio, A., Determination of the in vitro and in vivo antimicrobial activity on salivary streptococci and lactobacilli and chemical characterisation of the phenolic content of a *Plantago lanceolata* Infusion. Biomed Res. Int. vol. 2015, Article ID 286817, 8 pages, (2015). https://doi.org/10.1155/2015/286817
82. A.A. Sharifa, Y.L. Neoh, M.I. Iswadi, O. Khairul, M. Abdul Halim, M. Jamaludin, A.B. Mohamed Azman, H.L. Hing, Effects of methanol, ethanol and a aqueous extract of *Plantago major* on gram positive bacteria, gram negative bacteria and yeast. Ann. Microbiol. **8**, 42–44 (2008)
83. J.S. Kim, E. Kuk, K.N. Yu, J.H. Kim, S.J. Park, H.J. Lee, S.H. Kim, Y.K. Park, Y.H. Park, C.Y. Hwang, Antimicrobial effects of silver nanoparticles. Nanomed. Nanotechnol Biol. Med. **3**(1), 95–101 (2007). https://doi.org/10.1016/j.nano.2006.12.001

84. L. Zhang, Y. Jiang, Y. Ding, M. Povey, D. York, Investigation into the antibacterial behaviour of suspensions of ZnO nanoparticles (ZnO nanofluids). J. Nanopart. Res. **9**(3), 479–489 (2007). https://doi.org/10.1007/s11051-006-9150-1
85. C. Devatha, K. Jagadeesh, M. Patil, Effect of Green synthesized iron nanoparticles by *Azardirachta Indica* in different proportions on antibacterial activity. Environ. Nanotechnol Monit. Manag **9**, 85–94 (2018). https://doi.org/10.1016/j.enmm.2017.11.007
86. H. Sies, Oxidative stress: oxidants and antioxidants. Exp. Physiol. **82**(2), 291–295 (1997). https://doi.org/10.1113/expphysiol.1997.sp004024
87. C. Lee, J.Y. Kim, W.I. Lee, K.L. Nelson, J. Yoon, D.L. Sedlak, Bactericidal effect of zero-valent iron nanoparticles on *Escherichia coli*. Environ. Sci. Technol. **42**(13), 4927–4933 (2008). https://doi.org/10.1021/es800408u
88. M.S.H. Bhuiyan, M.Y. Miah, S.C. Paul, T.D. Aka, O. Saha, M.M. Rahaman, M.J.I. Sharif, O. Habiba, M. Ashaduzzaman, Green synthesis of iron oxide nanoparticle using *Carica papaya* leaf extract: application for photocatalytic degradation of remazol yellow RR dye and antibacterial activity. Heliyon. **6**, e04603 (2020). https://doi.org/10.1016/j.heliyon.2020.e04603

Figures

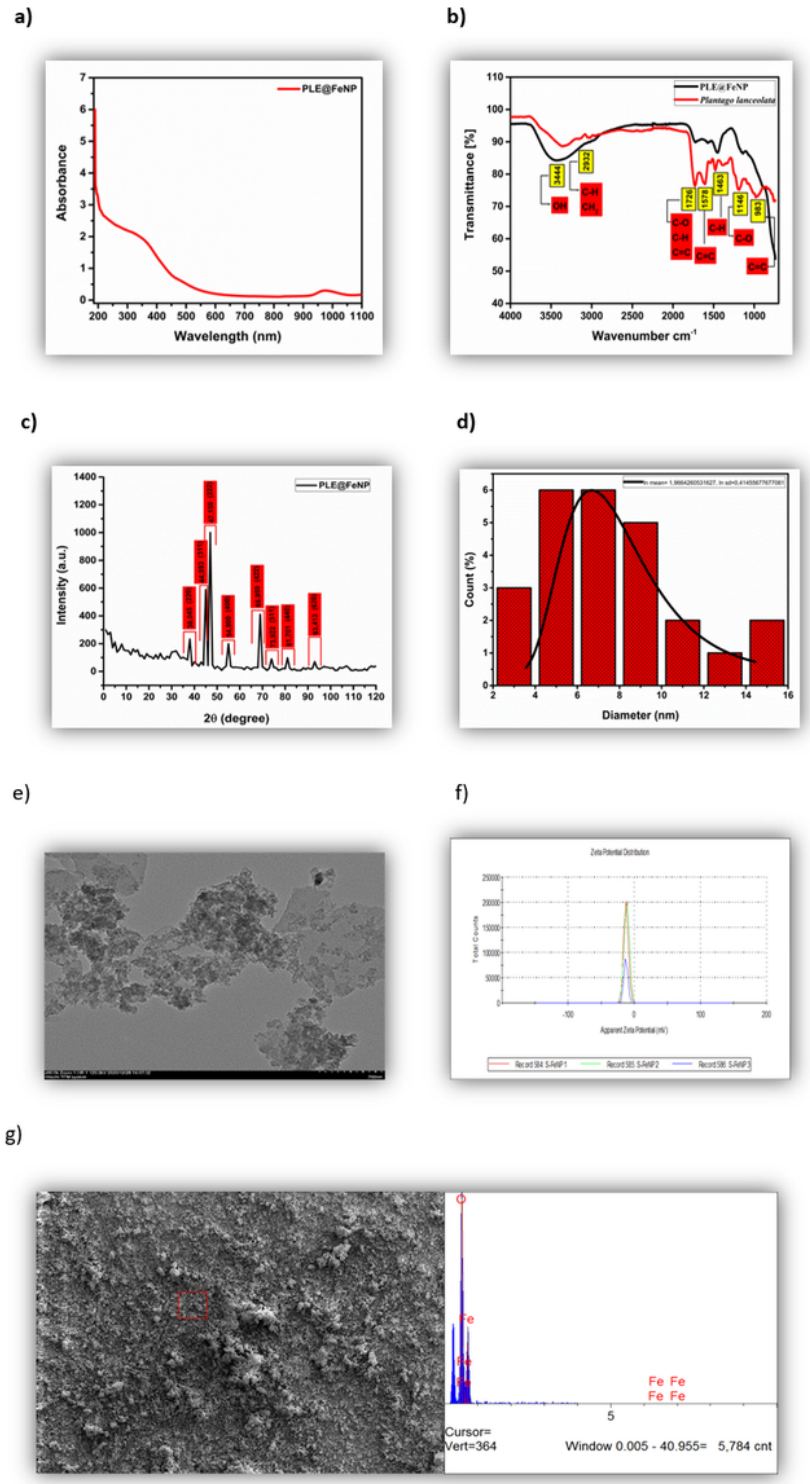

Figure 1

a) UV-spectrum 200-1100 cm-1 field scanning of PLE@FeNPs, **b)** FT-IR spectra of PLE@FeNPs, **c)** XRD graph of PLE@FeNPs, **d)** particle size distribution histogram., **e)** TEM analysis image of FeNPs biogenic synthesis, At 120 kv x60 k magnification, the bar size was scaled to 200 nm and the calculation was determined by the İmage J program **f)** Zeta potential plot of PLE@FeNPs. (g) SEM and EDX analysis results of PLE@FeNPs image of PLE@FeNPs. In the electron scattering presented by 5kV photons in

silver-plated samples, agromelaization of the PLE@FeNP system with Fe_3O_4 nanoparticles is observed at x 500 magnification. The bar size was measured as 50 µm at this magnification and small aggregations were observed. When the molecular weights of the atoms are examined, it is seen that the results overlap with Fe_3O_4. The high oxygen peak proves this. When the molecular weights of the atoms are examined, it is seen that the results overlap with Fe_3O_4. The high oxygen peak proves this.

First 0′

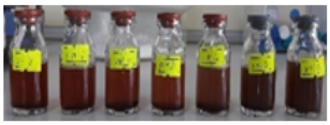

(a)

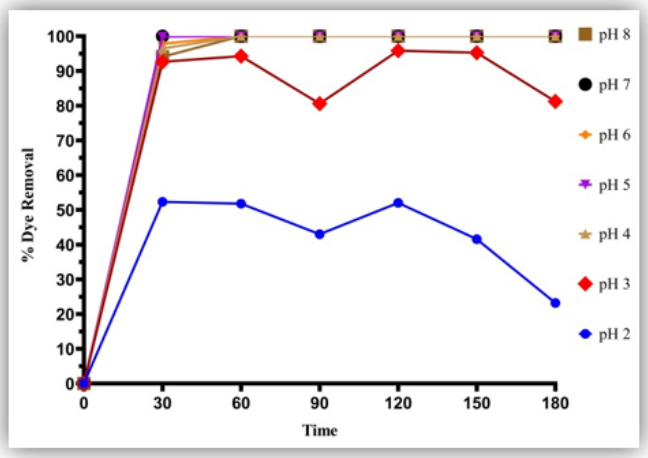

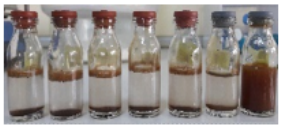

After 180′

First 0′

(b)

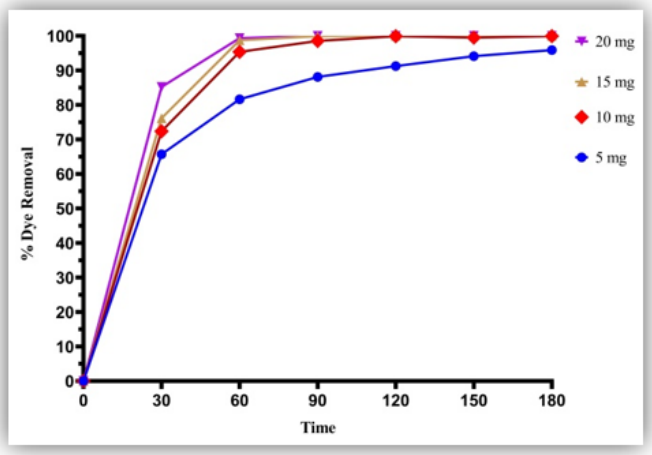

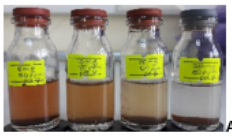

After 180′

Figure 2

a) pH scanning (pH 2–8) with 15 mg of PLE@FeNPs at 25 °C and 20 ppm dye concentration **b)** Congo red dye removal pH:8 with 5–20 mg of PLE@FeNPs and 50 ppm dye concentration.

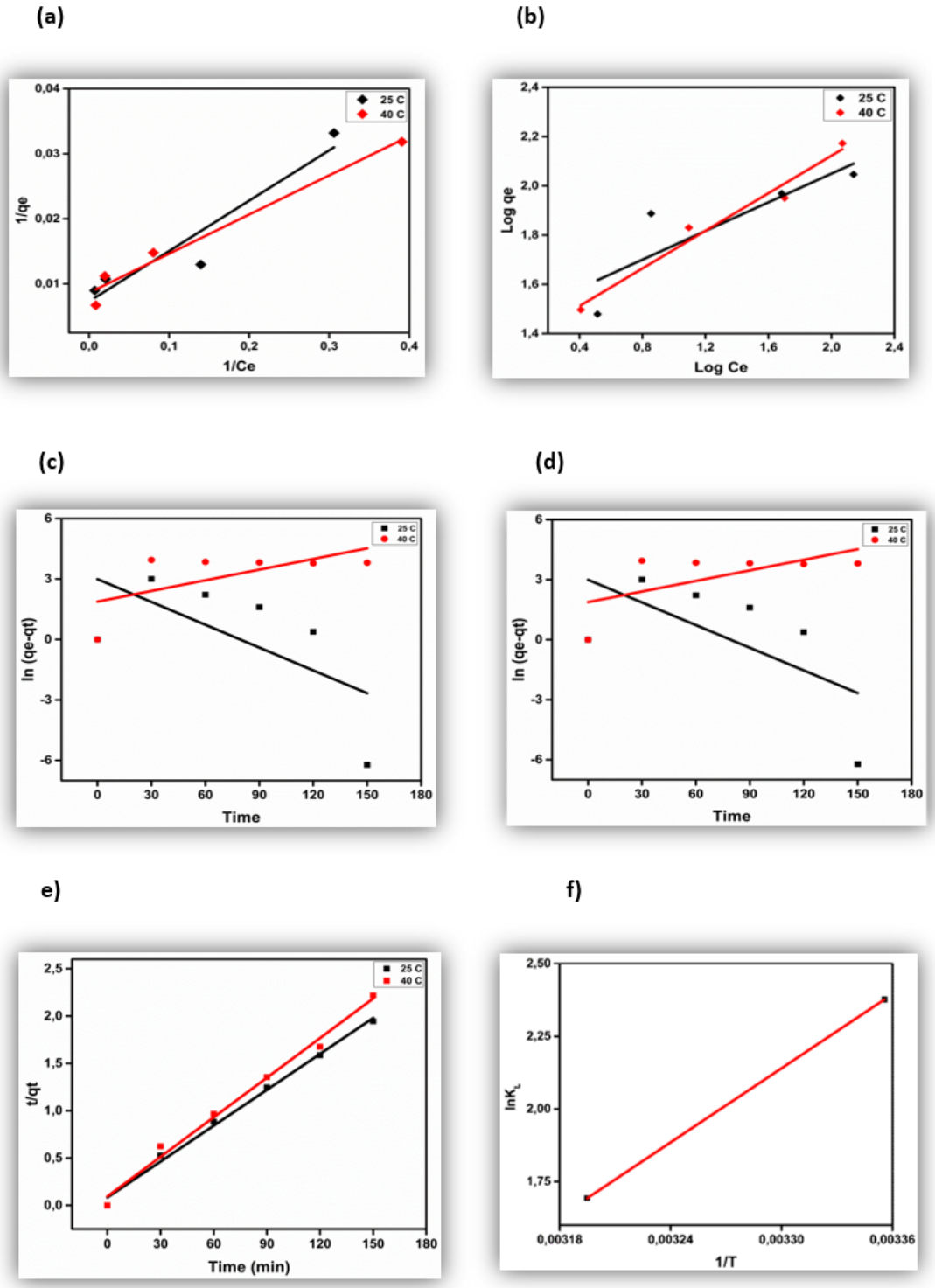

Figure 3

Plots of **a)** Langmuir isotherm, **b)** Freundlich isotherm, **c)** Temkin isotherm, **d)** Pseudo-first-order and **e)** pseudo-second-order plots for CR removal **f)** Graph showing the relationship between ln K_L and 1/T for CR removal with PLE@FeNPs.

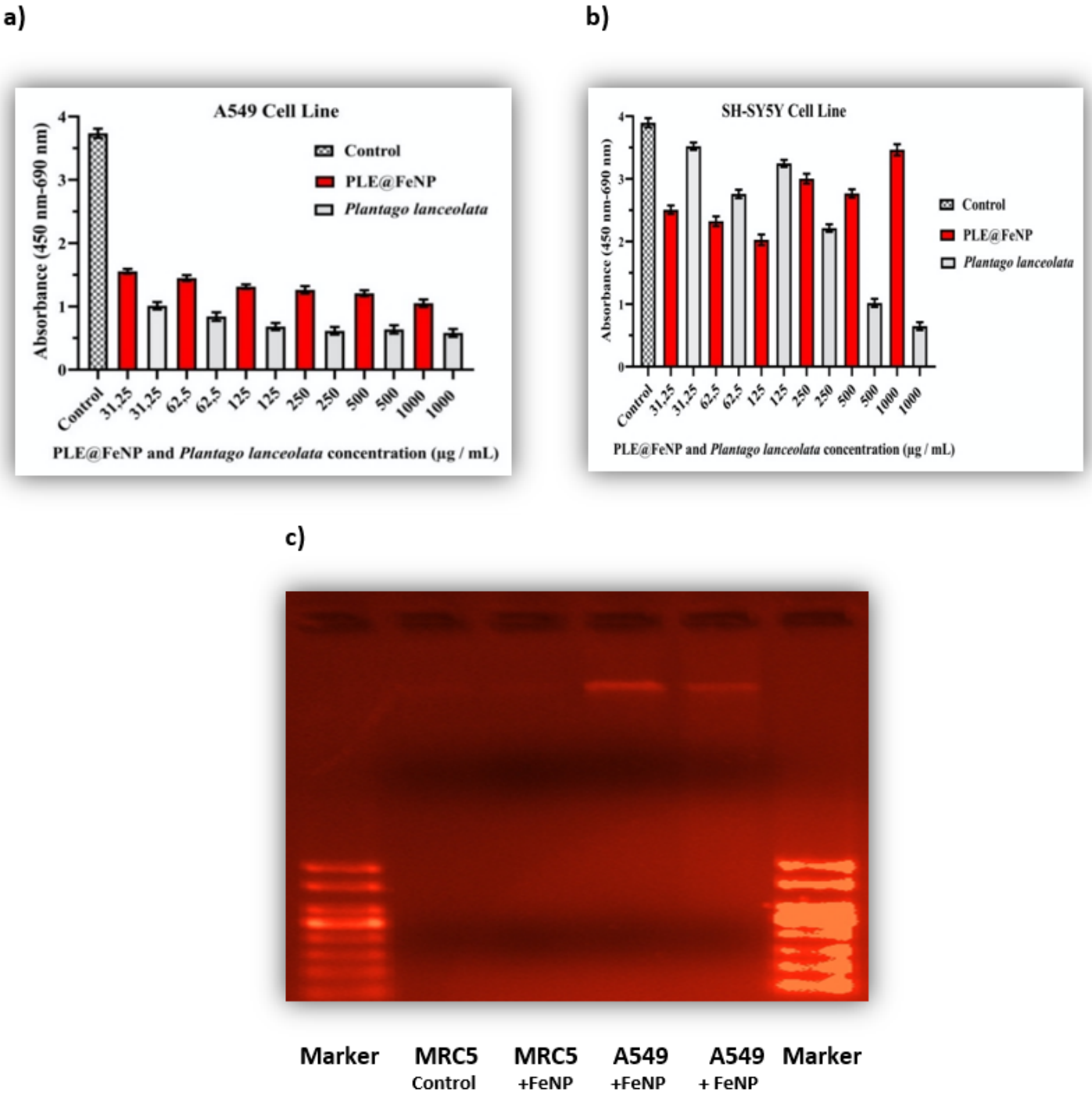

Figure 4

Graphs showing viability in cell lines A549 **(a),** SHSY5Y **(b)** after treatment with FeNPs and *P. lanceolata* plant water extract. Cell survival rates at concentrations obtained with serial dilutions in the range of 1000-31.25 µg/mL are given. Data mean ± SD of the study; N= 3, p-value < 0.01, **(c)** DNA fragmentation analysis of A549 and MRC-5

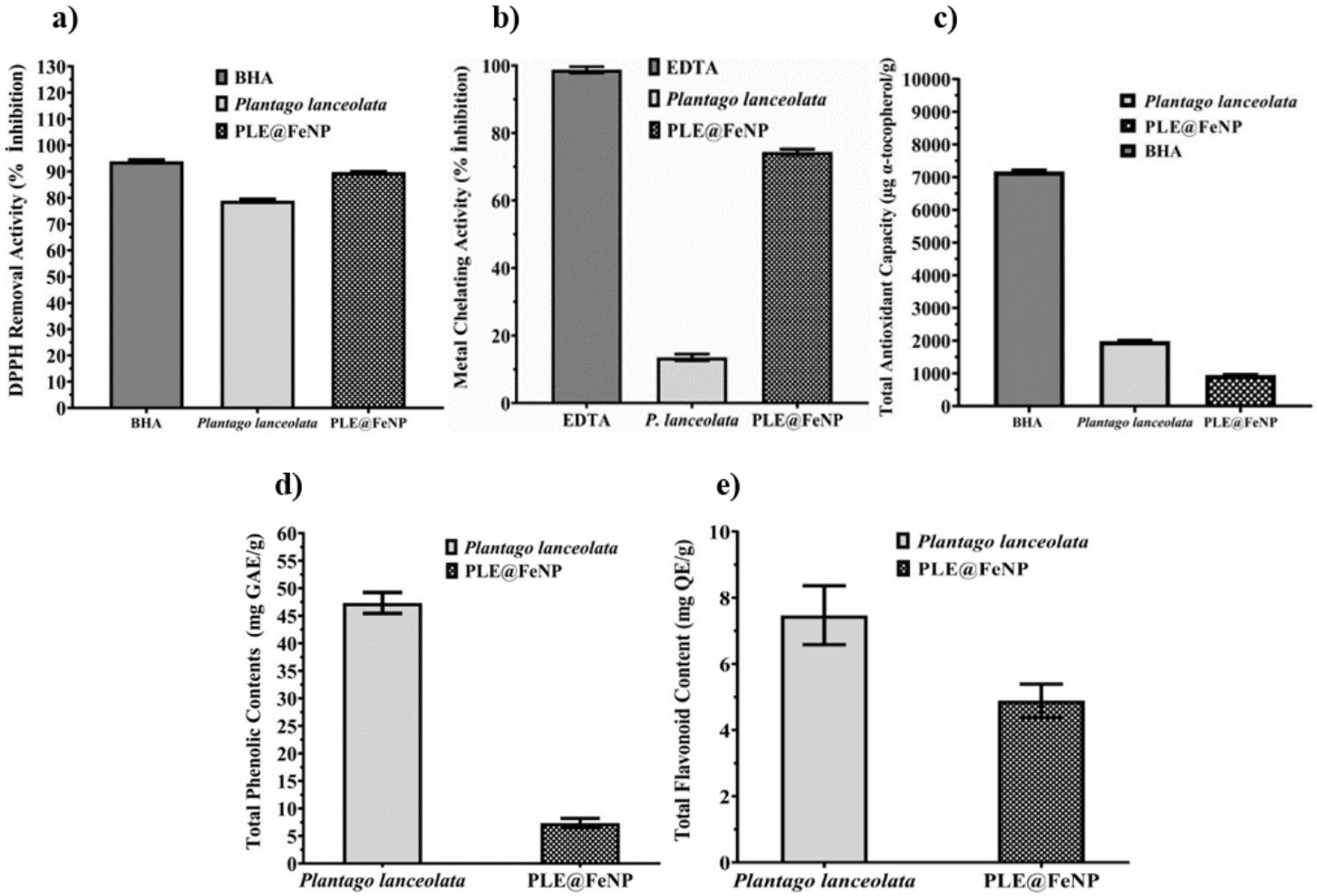

Figure 5

a) DPPH removal activity (% removal), **b)** metal chelating activity (% removal) **c)** Total antioxidant activity (µg α-tocopherol/g) **d)** total phenolic content (mg gallic acid/g) and **e)** total flavonoid content (mg quercetin /g). (Data mean ± SD of the studies; n= 3, p-value < 0.05.)

Supplementary Files

This is a list of supplementary files associated with this preprint. Click to download.

- GraphicalAbstract.png
- suplementarydata.docx